

# Journal of Materials Chemistry C

Accepted Manuscript



This is an *Accepted Manuscript*, which has been through the Royal Society of Chemistry peer review process and has been accepted for publication.

*Accepted Manuscripts* are published online shortly after acceptance, before technical editing, formatting and proof reading. Using this free service, authors can make their results available to the community, in citable form, before we publish the edited article. We will replace this *Accepted Manuscript* with the edited and formatted *Advance Article* as soon as it is available.

You can find more information about *Accepted Manuscripts* in the [Information for Authors](#).

Please note that technical editing may introduce minor changes to the text and/or graphics, which may alter content. The journal's standard [Terms & Conditions](#) and the [Ethical guidelines](#) still apply. In no event shall the Royal Society of Chemistry be held responsible for any errors or omissions in this *Accepted Manuscript* or any consequences arising from the use of any information it contains.

## ARTICLE

# Highly energy-efficient and air-stable organic transistors by an ultrathin hybrid dielectric with large internal voltage generation

Cite this: DOI: 10.1039/x0xx00000x

Received 00th January 2012,  
Accepted 00th January 2012

DOI: 10.1039/x0xx00000x

[www.rsc.org/](http://www.rsc.org/)Yu-Wu Wang,<sup>a</sup> Guan-Yi Tseng,<sup>a</sup> Liang-Yun Chiu,<sup>b</sup> Bo-Ren Lin,<sup>b</sup> Yu-Yang Lin,<sup>a</sup>  
Tsu-Wei Huang,<sup>a</sup> Wei-Yang Chou,<sup>b</sup> Lance Horng<sup>c</sup> and Horng-Long Cheng<sup>b,\*</sup>

This study presents an approach to designing hybrid dielectrics with ultrahigh capacitance density at extremely low supply voltages that behave like supercapacitors and are thus energy efficient. Hybrid dielectrics are fabricated from polymer/metal-oxide bilayer films with real-time and effective internal voltage generated by chemically interlocking interfacial species at the charged state. The designed dielectrics are named charged-state dipole-enhanced (CSDE) dielectrics. We demonstrate their potential use in ultralow voltage driving organic field-effect transistors (FETs) characterized by the high performance and great stability. Using the CSDE dielectrics, organic FETs with pentacene active layer can deliver adequate performance and excellent operational stability at ultralow operating voltage in ambient air. The linear field-effect mobility of pentacene-based FETs can be as high as 1.5 cm<sup>2</sup>/Vs at only 0.1 V. After long-term storage and continuous operations in air, the FETs still exhibited outstanding electrical performance. Several advantageous features of the designed CSDE dielectrics are presented, thereby providing a glimpse into the future of energy-efficient electronics.

## 1 Introduction

In recent years, the issue of energy-efficient and green technologies has received much attention.<sup>1</sup> The reduction in the power consumption of electric devices has become increasingly important, thus highlighting the importance of improving and expanding the application potential of such devices in electronics and photonics.<sup>2</sup> Dielectric materials of nanoscale dimensions have gained considerable interest and great importance not only in fundamental research but also in technological applications. These applications include nanocapacitors, nanobatteries, and other nanoscale electronics.<sup>3-5</sup> Development of nanodielectrics with excellent capacitance characteristics is highly demanded for various applications, especially for next-generation nano-scale and molecular-scale electronics. The most important example of an electric device is the field-effect transistor (FET), which is the basic element for integrated circuits having a wide range of applications from microelectronics, to optical displays as well as chemical and biological sensors.<sup>6,7</sup> An important trend in electronics is to obtain FET devices<sup>2,8</sup> with low power consumption operating at ultralow voltage with a rapid on/off switch, i.e., sharper subthreshold swing (*ss*) characteristics. Compared with inorganic semiconductor-based FETs, the development of ultralow voltage-driving organic FETs (OFETs) with high performance is faced with several major challenges: (i) Limited charge transport efficiency attributed to the lack of strong covalent bonds among organic molecules within a crystal/film results in the limited formation of delocalized electronic states.<sup>9</sup> (ii) An ultralarge driving voltage is needed to achieve

acceptable output currents when conventional gate dielectrics are used.<sup>10</sup> (iii) Electrical characteristics remain highly sensitive to organic structural orientations and defects, trap density and behavior, operating voltage, operating and stored environments, and so on.<sup>6,9-11</sup> An effective solution for reducing OFET operating voltages is to enrich charge accumulation by using materials with a high dielectric constant ( $\epsilon_r$ , also called high-K materials) as a gate dielectric.<sup>10</sup> However, OFETs using high-K gate dielectrics have been found to present several limitations, such as increased effective polaronic mass, broad density of states, and large densities of shallow traps at organic/dielectric interfaces with greater  $\epsilon_r$ .<sup>10,12-14</sup> Additionally, a gate dielectric that is highly compatible with organic semiconductors is essential for growing a high-quality active layer and, consequently, for achieving efficient charge transport within the active channel of OFETs.<sup>15,16</sup> Combining high-K nanodielectrics with self-assembled monolayers (SAM) to obtain hybrid gate dielectrics with high capacitance provides an alternative solution to low-voltage operation OFETs.<sup>10,17-21</sup> In particular, Klauk et al. reported ultralow-power organic complementary circuits based on OFETs with SAM gate dielectric.<sup>19</sup> Their SAM dielectrics exhibited excellent gate capacitance (0.7  $\mu\text{F}/\text{cm}^2$ ) and small leakage current (15 pA) with a thickness of only 2 nm, thus promoting ultralow-voltage OFETs with great electrical performance. Surface-modified cross-linked polymer films have been shown to offer great potential in obtaining low-voltage OFETs with good performance (e.g., saturated mobility as high as 3 cm<sup>2</sup>/Vs at 2 V).<sup>22</sup> Solid electrolytes as gate dielectrics that exhibit

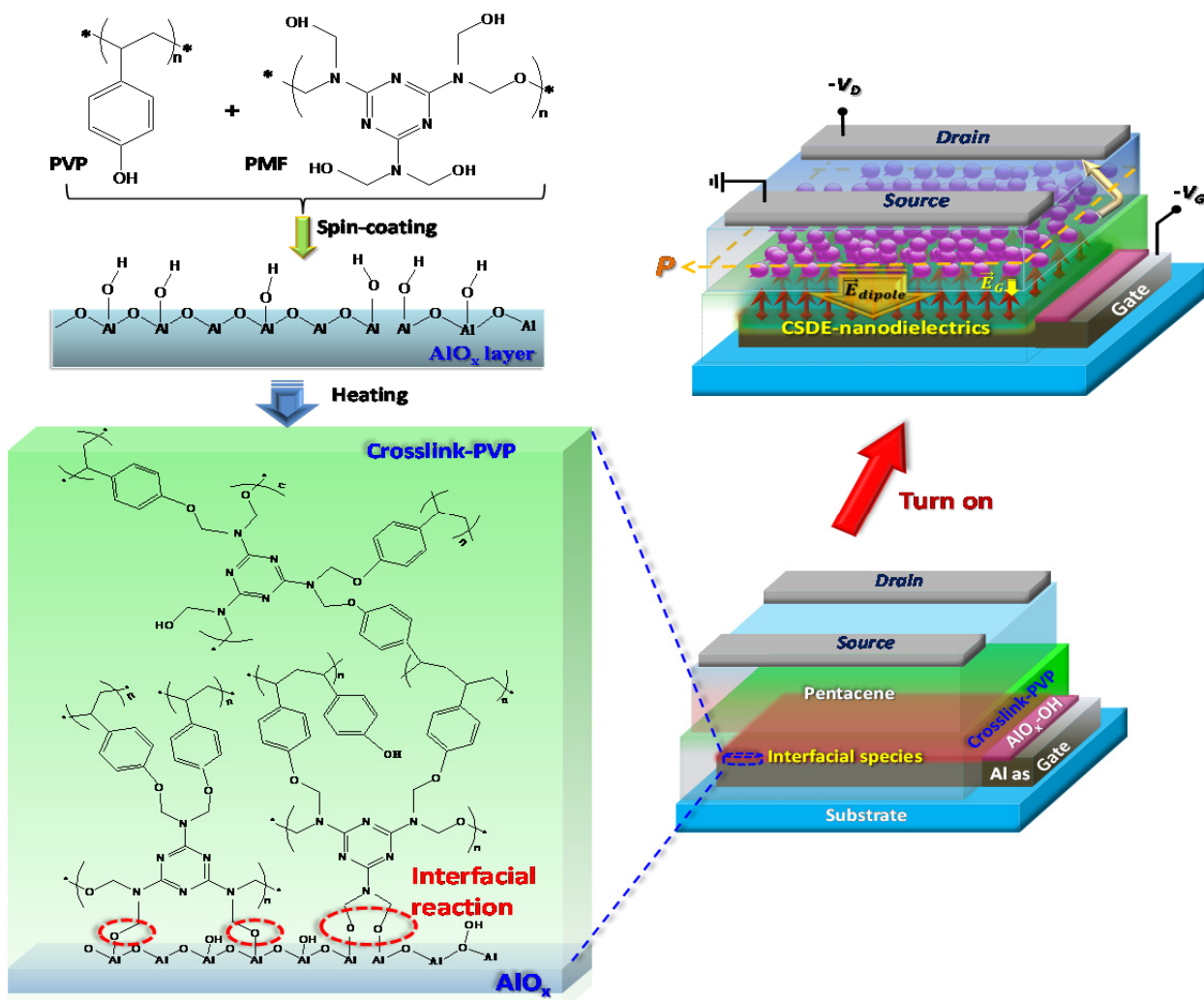


**Fig. 1** Schematic diagrams of pentacene OFET preparation with CSDE dielectric: (left panel) synthetic approach to CSDE dielectric based on a chemical reaction between the surfaces of  $\text{AlO}_x$ -OH, PMF, and PVP; (right panel) structure of fabricated bottom-gate top-contact OFETs. The applied external gate field ( $\vec{E}_G$ ) and internal dipole field ( $\vec{E}_{\text{dipole}}$ ) are shown during turn-on. Reference point P was used to calculate  $\vec{E}_{\text{dipole}}$ .

typically high capacitance ( $1 \mu\text{F}/\text{cm}^2$  to  $10 \mu\text{F}/\text{cm}^2$ ) has demonstrated a potential for use in low-voltage operations ( $< 2 \text{ V}$ ) of OFETs.<sup>23</sup> However, a major limitation of electrolyte gate dielectrics is that all materials in contact with the electrolyte must be electrochemically stable and corrosion-resistant. However, when capacitors are connected in a series, total capacitance is less than any of the individual capacitances of the capacitors in the series, thus resulting in another physical limit for lower driving voltage. Unless the aforementioned physical limitations are addressed, the further improvement of the electrical performance of OFETs at lower voltages (the best is below  $1 \text{ V}$ ) becomes increasingly difficult.

In this study, we present a novel concept of gate dielectrics with nanoscale dimensions that can generate a large real-time internal voltage (i.e., electric field) to aid in charge accumulation even with a very small given voltage. We utilized a high-reactivity oligomer poly(melamine-co-formaldehyde) (PMF, known as a cross-linking agent) to link the metal-oxide nanolayer and ultrathin insulating polymer layer, thus

producing hybrid bilayer nanoscale dielectrics with chemically interlocking interfaces and, more importantly, creating a specific interfacial molecule that can generate a large electric dipole moment in the charged state, as shown in Fig. 1. We aim to insert the electric dipole moments in the same direction as the gate field inside the dielectric, which is called the charged state dipole enhanced (CSDE) dielectrics in this work, to generate sufficient internal electric field at a very small input voltage (below  $0.5 \text{ V}$  and even down to  $0.1 \text{ V}$ ). The combination of polarization-electric field analysis and charge-enhanced Raman scattering with quantum chemical calculations offers unique opportunities for the direct exploration of embedded bottom interfacial species at charged states and for the detection of the magnitude of creation of internal electric fields. In contrast to methods using the electric dipoles of chemical moieties on the surface of gate dielectrics,<sup>12-14,21</sup> our approach uses the charged state electric dipoles of embedded interfacial molecules that can be readily provided to aid the

observation of ultralow voltage-driven OFETs with high performance and excellent operational stability in ambient air.

## II Results and discussion

Nanometer-scale metal-oxide dielectrics are directly formed at the bottom gate electrode through a simple oxygen plasma treatment performed on the metal electrode<sup>18,19</sup> (the gate electrode of OFETs). In this study, aluminum (Al) was used as an example. The formation of the AlO<sub>x</sub> nanolayer (about 4 nm, measured by ellipsometer) was verified through X-ray photoelectron spectroscopy (see ESI, Fig. S1†). After oxygen plasma treatment, the AlO<sub>x</sub> surface contained -OH and/or -O<sup>-</sup> surface active groups,<sup>19,22</sup> which facilitate the interfacial chemical reaction. A solution containing reactive PMF and poly(4-vinylphenol) (PVP) was spin-coated on the AlO<sub>x</sub> active surface to facilitate interfacial (PMF reacted with AlO<sub>x</sub>-O) and crosslink (PMF reacted with PVP) chemical reactions as illustrated in Fig. 1. After thermal heating, the bottom AlO<sub>x</sub> layer were chemically linked to the top crosslink-PVP layer with Al-O-C chemical bonds at the interface and thus hybrid dielectrics (< 40 nm) were formed. The thickness of top crosslink-PVP layer was only 30 ± 3 nm. Compared with the pristine AlO<sub>x</sub> nanolayer, the hybrid dielectric exhibited considerably improved leakage current resistance (ESI, Fig. S2a†). No evident breakdown within |bias| < 4 V is noted for the hybrid bilayer dielectrics. A corresponding dielectric strength of approximately 1 MV/cm in a leakage standard of 1 × 10<sup>6</sup> A/cm<sup>2</sup> was obtained, which guarantees that the corresponding OFETs work effectively under 4 V. However, some difficulty was experienced in the direct detection of interfacial molecules because the thickness of these molecules is only approximately 1 nm, and they are embedded at the bottom interface near the gate electrode. Combining in situ charge-enhanced Raman scattering and quantum chemical calculations provides an advanced approach for the detection of the formation of interfacial molecules between the AlO<sub>x</sub> layer and the crosslink-PVP layer (ESI, Fig. S3†). When a negative gate voltage (*V<sub>G</sub>*) was applied, we detected the Raman signals of Al-O-CH<sub>2</sub>-N-triazine vibrations of the interfacial molecules within the dielectrics because of the formation of the cation state. The formation of interfacial species makes CSDE dielectrics completely different from hybrid polymer/inorganic-oxide bilayer dielectrics.<sup>10</sup>

$\vec{P}$ - $\vec{E}$  analysis of different metal-insulator-semiconductor-metal (MISM) devices was conducted to investigate the electric dipole moments inside the dielectrics as well as the effects of these dipole moments on the charge accumulation of semiconductor.  $\vec{P}$ - $\vec{E}$  analysis allows for the further evaluation of the created electric dipole field. Examining the MIS capacitance and its dependence on externally applied voltages is important in OFET operations. Pentacene, a widely studied organic semiconductor in OFETs, was used as the semiconductor in this study. The present results were then compared with other results presented in the literature,<sup>17-21</sup> thereby revealing the benefits of the proposed application. Fig.

2 shows the  $\vec{P}$ - $\vec{E}$  curves of different MISM devices operating at various frequencies. Compared with other types of MISMs (discussed in detail below), the MISM with CSDE dielectrics exhibits unusual  $\vec{P}$ - $\vec{E}$  behavior, and the graph is asymmetrical to the origin. When  $-V_G$  is applied, a significantly enhanced electric susceptibility ( $\chi_e$ , i.e., slope of  $\vec{P}$ - $\vec{E}$  relationship, that is,  $\vec{P} = \chi_e \epsilon_0 \vec{E} = (\epsilon_r - 1) \epsilon_0 \vec{E}$ ,<sup>24</sup> where  $\epsilon_0$  and  $\epsilon_r$  are vacuum and relative permittivity, respectively), a nonlinear  $\vec{P}$ - $\vec{E}$  relationship, and counterclockwise hysteresis was observed. The aforementioned phenomena are evident at low operating frequency. The observed hysteresis can be attributed to the strong dependence of the dipole polarization on the history of the applied external  $\vec{E}$ , as observed in metal-ferroelectric-insulator-semiconductor diodes and contrary to the hysteresis developed by charge injection.<sup>25</sup> Furthermore, previous research on cross-linked PVP revealed that the unreacted hydroxyl groups inside of the film exhibits significant clockwise hysteresis behavior of capacitance-voltage (C-V) characteristics.<sup>26,27</sup> In this work, a reference HfO<sub>2</sub>/cross-linked PVP/pentacene MISM capacitor, in which the cross-linked PVP and the pentacene layers are made by using the same procedure, was tested and showed no considerable hysteresis behavior (Fig. 2b). Based on these observations, the conclusion is that the hysteresis observed in the MISM devices with CSDE dielectric is caused by the new interfacial dipole layer between cross-linked PVP and AlO<sub>x</sub>. Such counterclockwise hysteresis behavior in C-V outputs can also be observed in the corresponding MIM devices (ESI, Fig. S2b†).

For the dielectric without permanent and switchable internal dipoles (i.e., a linear capacitor), the induced  $\vec{P}$  was proportional to  $\vec{E}$ . The theoretical curve in the  $\vec{P}$ - $\vec{E}$  graph can simply be determined by  $\epsilon_r$ . As observed in the silicon dioxide (SiO<sub>2</sub>) and pentacene MISM case (Fig. 2b), the experimental curve was highly correlated with the theoretical prediction and symmetrical to the origin. However, the presence of dipoles in a polarizable medium would result in an increase in the  $\epsilon_r$  and thus  $\chi_e$  according to the Debye equation,<sup>28</sup>

$$\frac{\epsilon_r - 1}{\epsilon_r + 2} = \frac{\rho}{3\epsilon_0} \left( \frac{\mu_D^2}{3k_B T} + \alpha \right) \quad (1)$$

where  $\rho$  is the density of the dipole,  $\mu_D$  is the permanent electric dipole,  $\alpha$  is the polarizability,  $k_B$  is the Boltzmann constant, and  $T$  is the temperature. An observation of the  $\vec{P}$ - $\vec{E}$  relationship in Fig. 2a indicates that the large dipole effects within the MISM with CSDE dielectrics only occur under a negative  $\vec{E}$ . Moreover, the observed frequency-dependent slope in the  $\vec{P}$ - $\vec{E}$  graph is evidence of the time-dependent dipole response.

Quantum chemical calculations of the  $\mu_D$  of the interfacial molecule in various situations were performed to interpret the unusual  $\vec{P}$ - $\vec{E}$  graph of CSDE dielectrics. In the neutral state, the calculated  $\mu_D$  was only 0.3 D; the symmetry of the molecular geometry was maintained. After applying downward (-) and upward (+)  $\vec{E}_G$  of 5.1 × 10<sup>5</sup> V/cm (equivalent to  $V_G = -2$  V or +2 V in real OFETs, respectively), the observed  $\mu_D$  are only

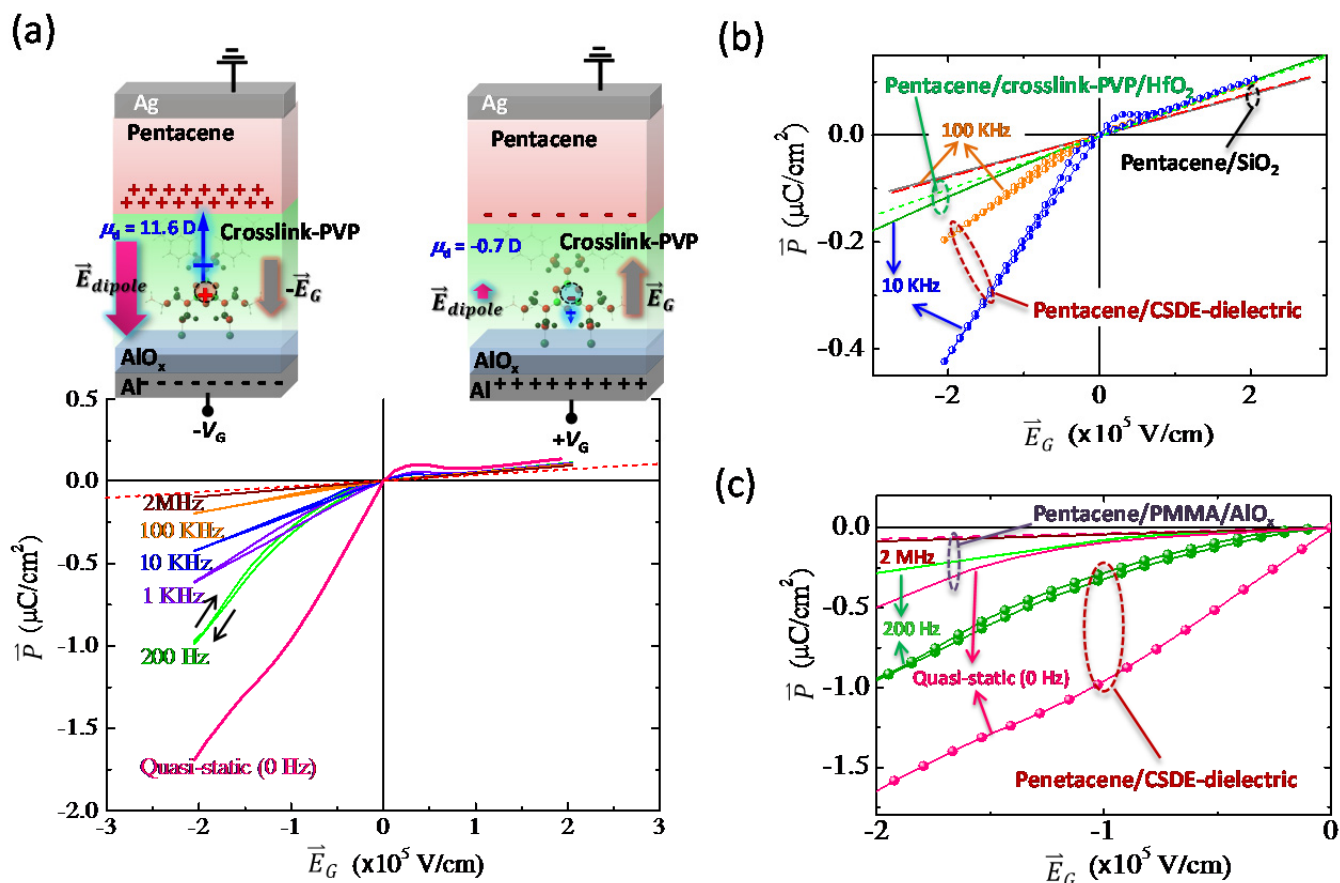


**Fig. 2** Polarization ( $\bar{P}$ ) versus applied gate electric fields ( $\bar{E}_G$ ) of pentacene-based MISMDiodes using different dielectrics: (a) CSDE dielectric, (b) SiO<sub>2</sub> and crosslink-PVP/HfO<sub>2</sub> dielectrics, and (c) PMMA/AIO<sub>x</sub> dielectric. The solid lines show the experimental curves obtained from various frequencies. The dashed lines show the theoretical curves from the total dielectric constants ( $\epsilon_r$ ) obtained according to the total capacitance of capacitors in series; this total capacitance is equal to the reciprocal of the sum of the reciprocals of the individual capacitances. The  $\epsilon_r$  of the AIO<sub>x</sub>, crosslink-PVP, SiO<sub>2</sub>, HfO<sub>2</sub>, and PMMA was 6.1, 3.9, 3.9, 10.0, and 3.5, respectively, according to capacitance–voltage measurements. The  $\epsilon_r$  of pentacene was 3.92 according to ref. (29). The inset in (a) illustrates the internal dipole field ( $\bar{E}_{dipole}$ ) evolutions of the interfacial dipole moment ( $\mu_d$ ) when the devices were operated at different regimes. The applied gate voltage ( $V_G$ ) and the corresponding  $\bar{E}_G$  are shown. For comparison, the curves (circle symbols) of the pentacene/CSDE dielectric-based devices operated at the same frequency are also shown in (b) and (c).

0.43 D and 0.15 D, respectively. However, when an external  $\bar{E}$  was applied, the interfacial molecules within the dielectric were charged because of dielectric polarization. When  $-V_G$  was applied, the interfacial molecule had a positive charge. The resultant  $\mu_d$  values of the interfacial molecule in the cation state increased considerably to 11.4 D. The observed  $\mu_d$  values increased slightly to 11.6 D after the application of  $-\bar{E}_G$  of  $5.1 \times 10^5$  V/cm. When  $+V_G$  was applied, the molecule acquired a negative charge, and the resultant  $\mu_d$  values were only  $-0.6$  and  $-0.7$  D, with or without  $+\bar{E}_G$  of  $5.1 \times 10^5$  V/cm (inset of Figure 2a, right panel). Despite the significant dependence of the initial  $\mu_d$  on the molecular geometry, a very large  $\mu_d$  can be created only in the molecule with a positive charge, i.e., the cation state. The theoretical calculations indicate that a significant change in electron density distribution occurred at the cation state, thus generating a large  $\mu_d$ . The highest occupied molecular orbital (HOMO) was found at the  $-N-C-O-PVP$  side. By contrast, the HOMOs of the neutral and anion

states were located at the  $-N-C-O-Al$  side. The lowest unoccupied molecular orbitals were mainly located at the  $-N-C-O-Al$  side and were found to be insensitive to the charge state. The unusual  $\bar{P} - \bar{E}$  behavior in Figure 2a can be reasonably attributed to the large  $\mu_D$  of the interfacial species only at the cation state. By contrast, the contributions of the electric field-induced polarization  $\alpha$  of the interfacial species are not critical.

The dipoles were aligned during the measurements, creating an internal dipole field ( $\sum \bar{E}_{dipole}$ ) that could enhance or diminish the applied external  $\bar{E}_G$ . When operated at  $+V_G$  and  $-V_G$ , the net electric field ( $\bar{E}_{net}$ ) can be expressed as follows:

$$\text{for } V_G > 0 \text{ V, } |\bar{E}_{net}| = |\bar{E}_G| - |\sum \bar{E}_{dipole(0)}| + |\sum \bar{E}_{dipole(-)}| \quad (2)$$

$$\text{for } V_G < 0 \text{ V, } |\bar{E}_{net}| = |\bar{E}_G| + |\sum \bar{E}_{dipole(0)}| + |\sum \bar{E}_{dipole(+)}| \quad (3)$$

where subscripts (0), (-), and (+) correspond to the dipole field from the neutral, anion, and cation states, respectively. For position  $P$  along the dipole axis (Fig. 1), the internal dipole field can be calculated simply by

$$\sum \vec{E}_{dipole} = \frac{l\mu_d}{2\pi\epsilon_0 R^3} \times n \quad (4)$$

where  $l$  is the dipole length,  $R$  represents the distance between the dipole and point  $P$ , and  $n$  is the number of dipoles. Effective  $|\vec{E}_{net}|$  that contributes to charge accumulation can be estimated from the  $\vec{P}$ - $\vec{E}$  graph through linear extrapolation of the theoretical curve at the same polarization density, thereby obtaining internal fields ( $E_{int}$ ) by subtracting  $|\vec{E}_G|$  from  $|\vec{E}_{net}|$ . All the internal fields (including the field of the image dipole) that contribute to polarization are included in this approach. At  $V_G$  of  $-0.5$  and  $-2$  V, the observed  $E_{int}$  reached as high as  $-1.4 \times 10^6$  (equivalent to  $V_G$  of  $-13.8$  V) and  $-4.6 \times 10^6$  V/cm (equivalent to  $V_G$  of  $-45$  V) through quasi-static measurements (see Fig. 3a). However, even at  $V_G$  of  $+2$  V, the observed  $E_{int}$  was only  $2.0 \times 10^5$  V/cm (equivalent to  $V_G$  of  $1.9$  V) (Fig. 3b). We noted that the presence of charge-trapping effects results in the underestimation of  $E_{int}$ , as the case of pentacene/SiO<sub>2</sub> device. Assuming that  $E_{int}$  was dominated by the dipole field from the interfacial molecules, the  $\mu_d$  ratio of the cation to anion state at different  $V_G$  can be further calculated by eqn (1) given that  $l$ ,  $n$ , and  $R$  have similar values. The observed  $\mu_d$  ratio of the cation to anion state at  $|V_G|$  of  $0.8$  V to  $1.0$  V was close to the theoretical prediction, which is approximately 17.

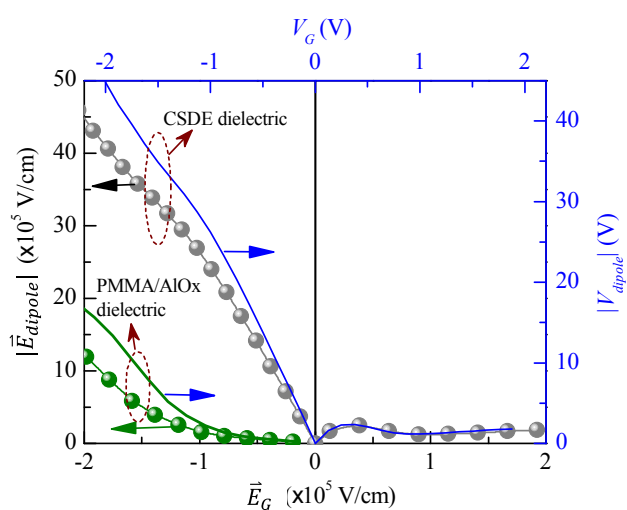


**Fig. 3** Internal dipole electric field ( $\vec{E}_{dipole}$ , which corresponds to  $V_{dipole}$ ) as a function of the external gate electric field ( $\vec{E}_G$ , which corresponds to  $V_G$ ) of pentacene-based MISD diodes using the CSDE and PMMA/AIOx dielectrics, respectively.

By contrast, the dipole effects of the AlO<sub>x</sub> layer, crosslink-PVP layer, pentacene layer, pentacene/crosslink-PVP interface, and other incorporated dipoles can be excluded by comparing the  $\vec{P}$ - $\vec{E}$  relationship of different MISD devices, such as

pentacene/SiO<sub>2</sub> (Fig. 2b), pentacene/crosslink-PVP/HfO<sub>2</sub> (Fig. 2b; the case allows for the examination of the dipole effects of the crosslink-PVP layer, the pentacene layer, and the interface between crosslink-PVP and pentacene), and pentacene/poly(methyl methacrylate) (PMMA)/AlO<sub>x</sub> [Fig. 2c; a PMMA layer with similar thickness (approximately 25 nm) was used to replace the crosslink-PVP layer in the hybrid bilayer dielectrics to enable the examination of the dipole effects of the AlO<sub>x</sub> layer and polar functional groups of the polymer insulator layer], with the present CSDE dielectric devices. The randomly incorporated dipole has no fixed direction, i.e., it has random orientations. Thus, the dipole effect was not effectively observed at low electric fields and high frequencies, such as in the cases of pentacene/PMMA/AlO<sub>x</sub> and pentacene/crosslink-PVP/HfO<sub>2</sub>. The theoretical calculations also indicate that the dipole direction of Al-OH on the surface of AlO<sub>x</sub> is in the wrong direction, which diminishes the applied  $-\vec{E}_G$ . These results differ from those obtained by CSDE dielectrics.

The electrical characteristics of pentacene OFETs with CSDE dielectrics under ambient air conditions (Fig. 4) were then investigated. The electrical performance of OFETs is not a simple function of the amount of accumulated charges in the active channel. Such performance is also highly dependent on the microstructural quality of the organic semiconductors, surface properties of dielectrics, and interfacial trap density.<sup>6,9-11,30-32</sup> OFETs with PMMA/AlO<sub>x</sub> dielectrics were used as a reference sample to minimize or eliminate other factors. The PMMA surface properties (with a surface roughness of approximately 5 Å and surface energy of approximately 46 mJ/m<sup>2</sup>) are similar to those of the crosslink-PVP surface; thus, both are suitable for the deposition of high-quality pentacene films (ESI, Fig. S4†). The factors that affect the microstructural properties of organic semiconductor and interface roughness scattering on charge transport within the active channel can be minimized.<sup>30-32</sup> Pentacene grown on a PMMA buffer layer exhibits a high mobility of above 1.0 cm<sup>2</sup>/V·s at high bias ( $-40$  V, equivalent to  $\vec{E}$  larger than  $10^6$  V/cm); these properties are attributed to the good charge transport-related microstructural features of pentacene on PMMA.<sup>16,33</sup> The PMMA system has disordered electric dipoles owing to its amorphous nature. High electric fields are required to align these dipoles and to obtain a useful dipole field (Figs. 2c and 3a). A threshold  $\vec{E}$  of ca.  $10^5$  V/cm of the PMMA was observed. Furthermore, the pentacene/PMMA interface has relatively low interfacial trap density ( $D_{it}$ ) compared with the pentacene/crosslink-PVP interface (ESI, Fig. S5†). Based on this information, the remarkable effects of the internal electric dipole field on approaching ultralow-voltage OFETs with outstanding performance can be highlighted. The output current ( $I_{DS}$ ) generated by the OFETs with CSDE dielectrics is more than 300 times greater than that produced by the PMMA/AlO<sub>x</sub> devices (Fig. 4a) despite the large  $D_{it}$  ( $9.3 \times 10^{11}$  1/eV·cm), which is approximately twice as large as that in the PMMA case ( $4.8 \times 10^{11}$  1/eV·cm). The field-effect mobilities in the linear ( $\mu_{lin}$ ) and saturation ( $\mu_{sat}$ )

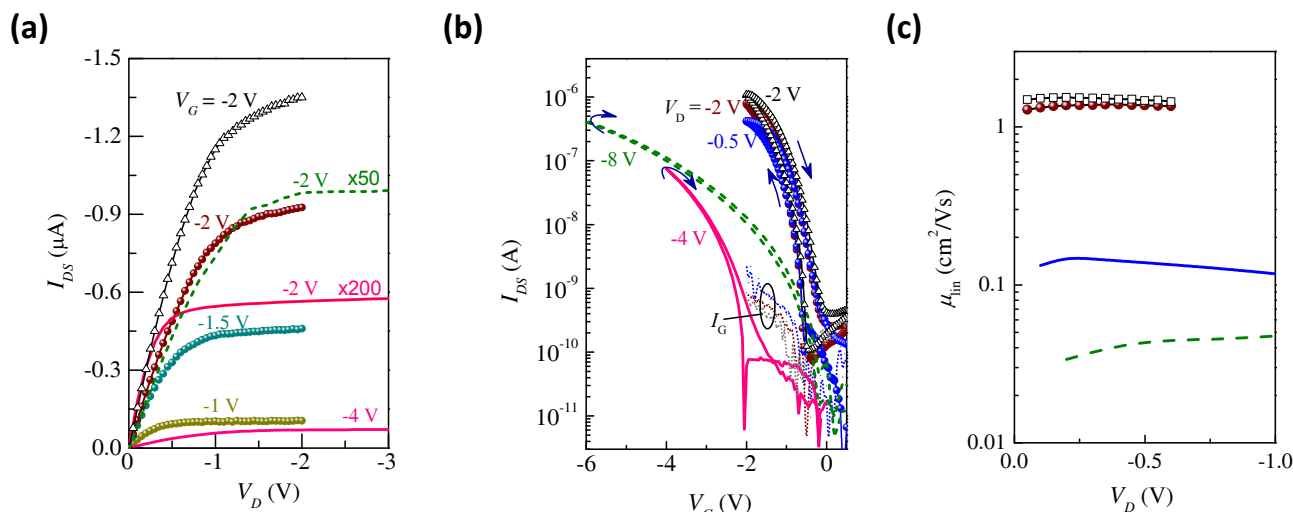


**Fig. 4** Electrical characteristics of pentacene-based OFETs employing different gate dielectrics with selected channel lengths ( $L$ ): CSDE dielectric (cycles,  $L$  of 250  $\mu\text{m}$ ); PMMA/ $\text{AlO}_x$  dielectric (solid lines,  $L$  of 250  $\mu\text{m}$ ); crosslink-PVP/ $\text{HfO}_2$  dielectric (dashed lines,  $L$  of 100  $\mu\text{m}$ ). (a) Output characteristics [drain current ( $I_{\text{DS}}$ ) as a function of drain-source voltage ( $V_{\text{D}}$ ) at selected gate voltage ( $V_{\text{G}}$ )]. (b) Transfer characteristics ( $I_{\text{DS}}$  as a function of  $V_{\text{G}}$  at selected  $V_{\text{D}}$ ). The arrows indicate the sweep direction of  $V_{\text{G}}$ . Gate currents ( $I_{\text{G}}$ ) as a function of  $V_{\text{G}}$  are also shown for OFET with CSDE dielectric. (c) Linear field-effect mobility ( $\mu_{\text{lin}}$ ) as a function of  $V_{\text{D}}$  biases. The  $\mu_{\text{lin}}$  was obtained using the transconductance method. OFETs using CSDE dielectric with different  $L$  values (triangles: 100  $\mu\text{m}$ ; squares: 300  $\mu\text{m}$ ) operating at selected voltages are shown for comparison.

regions of pentacene OFETs with CSDE dielectrics were 2.0  $\text{cm}^2/\text{V}\cdot\text{s}$ . These mobilities obtained from the transfer curves had an average of 1.6  $\text{cm}^2/\text{V}\cdot\text{s}$  to 1.9  $\text{cm}^2/\text{V}\cdot\text{s}$  based on at least 15 devices. The  $\mu_{\text{lin}}$  values are close to the  $\mu_{\text{sat}}$  values unlike most pentacene-based OFETs reported in literature.<sup>6,34</sup> The devices exhibited a relatively high  $\mu_{\text{lin}}$  of 1.5  $\text{cm}^2/\text{V}\cdot\text{s}$  at a drain bias ( $V_{\text{D}}$ ) of only  $-0.1$  V (Fig. 4c). Conversely, the  $\text{AlO}_x/\text{PMMA}$  devices displayed a relatively low  $\mu_{\text{lin}}$  and  $\mu_{\text{sat}}$  values (below 0.2  $\text{cm}^2/\text{V}\cdot\text{s}$ ) when operated at  $V_{\text{D}}$  of  $-0.5$  and  $-4$  V, respectively. The observed threshold voltage ( $V_{\text{th}}$ ) of  $-2.2$  V ( $\pm 0.35$  V) was large. The obtained mobilities are similar to the results reported by Shang et al., who operated pentacene OFETs with a PMMA-modified  $\text{AlO}_x$  gate dielectric at  $-3$  V.<sup>35</sup> Furthermore, in the absence of a considerably effective  $\sum \vec{E}_{\text{dipole}}$ , pentacene OFETs with crosslink-PVP/ $\text{HfO}_2$  bilayer dielectrics only exhibit fair electrical characteristics (Fig. 3;  $\mu_{\text{sat}}$  of 0.1  $\text{cm}^2/\text{V}\cdot\text{s}$  even when operated at  $-8$  V and  $\mu_{\text{lin}}$  below 0.06  $\text{cm}^2/\text{V}\cdot\text{s}$ ); these results may be attributed to the large  $D_{\text{it}}$ .

Several supplementary experiments were also conducted to better understand the CSDE dielectrics. Different process conditions of crosslink-PVP were tested by changing the solution concentrations, spin-coating conditions, and the PVP:PMF weight ratio. The optimized concentration of PVP and PMF was only 1 wt%; this value is lower than that in other previous studies on crosslink-PVP.<sup>26,27,36-39</sup> A significant decrease in the electrical performance was observed when thick crosslink-PVP layers, prepared from a high-concentration solution, were used in the CSDE dielectrics (ESI, Fig. S6†). These results are in agreement with the forecast from eqn (4), where  $|\sum \vec{E}_{\text{dipole}(+) }|$  is inversely

proportional to  $R^3$ , that is, the thickness of the crosslink-PVP. Afterward, OFETs with pristine PVP films and with  $\text{AlO}_x$  as the gate dielectric (without adding PMF, thus lacking in interfacial species) were also tested. The devices also exhibited inferior electrical performance (ESI, Fig. S7†). Water molecules were adsorbed because a pure PVP film contains a large amount of hydroxyl groups at the surface and inside the film in the absence of a crosslink; this condition affected the electrical properties.<sup>26,27,36</sup>

We also examined the hysteresis behaviors of OFETs (Fig. 4b). This hysteresis voltage is defined as the  $V_{\text{th}}$  between forward and reverse scans. OFETs with CSDE dielectric exhibit hysteresis voltage of  $0.028 \pm 0.03$  V larger than that generated by devices with PMMA/ $\text{AlO}_x$  and crosslink-PVP/ $\text{HfO}_2$  dielectrics. The clockwise hysteresis direction agrees with most observations for pentacene OFETs with a polymer buffer layer or dielectrics, a direction attributed to the slow polarization of polar functional groups.<sup>26,27,40</sup> In contrast, a charge-trapping mechanism has reasonably explained the counterclockwise hysteresis in pentacene OFETs.<sup>41</sup> Moreover, the counterclockwise hysteresis in pentacene OFETs using PVP/silicon dioxide dielectrics is observed in ambient air because water diffuses into the active channel,<sup>36</sup> which allows the water issue to be excluded in this work. Overall, the observed clockwise hysteresis phenomena of OFETs with CSDE dielectric is reasonably attributed to polarization effects from an interfacial dipole moment.

The capacitance–frequency ( $C$ - $F$ ) characteristics of the MIM diodes with CSDE dielectrics were also assessed (Fig. 5a). The observed  $\epsilon_r$  was above 8.0 at a frequency below 40 KHz. This value is unusually high compared with previous

results for a single layer of  $\text{AlO}_x$  ( $\epsilon_r$  of 6.2–6.5),<sup>18,37,38</sup> crosslink-PVP ( $\epsilon_r$  of approximately 3.6–4.0),<sup>38,42</sup> and generally, crosslink-PVP combined with  $\text{AlO}_x$  ( $\epsilon_r$  of ca. 4.0–4.3).<sup>37,38</sup> The high  $\epsilon_r$  value confirms the presence of internal dipole fields that enhance total electric field strength and yield high capacitance. Consequently, decrease in  $\epsilon_r$  as the thickness of the cross-linked PVP layer increases is also observed in the CSDE dielectric (ESI, Fig. S6c†). With the same measurement methods and device dimensions, MIM with PMMA/ $\text{AlO}_x$  dielectrics exhibited reasonable  $\epsilon_r$  (i.e., 3.7 at 40 KHz). In Fig. 5a,  $\epsilon_r$  slightly increases with decreased frequency, a common polymer dielectric feature caused by the slow polarization of polar functional groups.

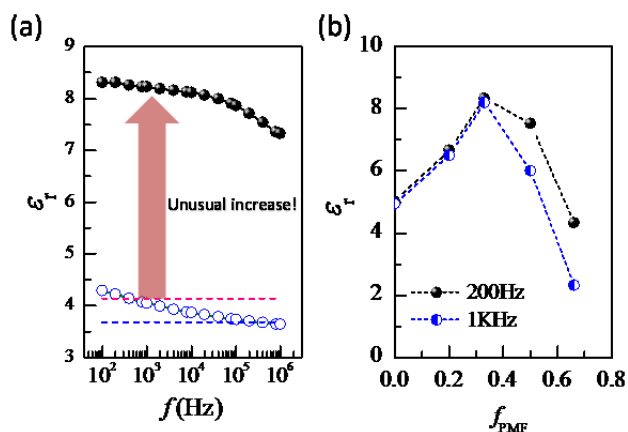


**Fig. 5** (a) The dielectric constant ( $\epsilon_r$ ) varies as a function of frequency ( $f$ ) for the CSDE dielectric (solid symbols) and PMMA/ $\text{AlO}_x$  dielectric (open symbols). The  $\epsilon_r$  was determined from the measurements of the capacitance in a MIM configuration with an electrode area of  $0.0015 \text{ cm}^2$ . Dashed lines show the theoretical  $\epsilon_r$  values, which are obtained according to the formula for series capacitance. For the  $\text{AlO}_x$ , crosslink-PVP, and PMMA, the  $\epsilon_r$  values were taken as 6.1, 3.9, and 3.5, respectively, by capacitance–voltage measurements. (b) The  $\epsilon_r$  values as a function of the given weight fraction of PMF ( $f_{\text{PMF}}$ ) for pristine PVP/ $\text{AlO}_x$  and crosslink-PVP/ $\text{AlO}_x$  dielectrics, respectively.

The effect of PVP:PMF weight ratio on the dielectric properties of CSDE dielectrics is investigated, and the results are summarized in Fig. 5b. Without adding the cross-linking agent, the observed  $\epsilon_r$  values of pristine PVP on  $\text{AlO}_x$  of 5.0 are similar to the values reported elsewhere.<sup>36,42</sup> With the addition of PMF, the maximum value of  $\epsilon_r$  of the dielectrics was found in the sample with a PVP:PMF ratio of 2:1, which is notably very close to the theoretical value, to obtain a fully cross-linked PVP layer. The  $\epsilon_r$  values rapidly decrease with the addition of excess PMF. The dielectric does not work properly when the PMF weight fraction ( $f_{\text{PMF}}$ ) is greater than 0.7 because of large leakage currents (ESI, Fig. S2a†). Moreover, the observed relationship between the  $\epsilon_r$  values and the PVP:PMF weight ratio is completely different from that of the cross-linked PVP single layer, in which the  $\epsilon_r$  values decrease with increasing PMF ratio.<sup>43</sup> Meanwhile, the pristine PVP films exhibit higher  $\epsilon_r$  values than those of the cross-linked ones owing to the presence of hydroxyl groups.<sup>36,43</sup> An abnormal increase of  $\epsilon_r$  in ambient air is also reported in

pristine PVP films and is attributed to water molecules absorbed and diffused into the film because of the hydroxyl groups.<sup>36</sup> In this study, pristine PVP, cross-linked PVP ( $f_{\text{PMF}}$  of 0.2), and cross-linked PVP ( $f_{\text{PMF}}$  of 0.66) on the  $\text{AlO}_x$  with excess hydroxyl groups from either PVP or PMF exhibited increased  $\epsilon_r$  values from a nitrogen to a humid atmosphere (RH above 80%), from 4.0, 5.2, and 2.0 to 5.0, 6.1, and 4.3 (at 200 Hz), respectively. By contrast, the sample with a 2:1 ratio did not exhibit a decrease in  $\epsilon_r$  under a nitrogen atmosphere (e.g.,  $\epsilon_r$  value of approximately 8.5 at 300 Hz). Accordingly, the internal dipole fields contributed by the residual hydroxyl groups can be ignored under the optimized CSDE dielectrics. Furthermore, the  $\epsilon_r$  of the CSDE dielectrics remains constant even after long-term post-annealing treatments. The result seems quite reasonable considering that the present cross-linked PVP layer is very thin (typically only 30 nm), such that the curing reaction is easily completed.<sup>44</sup>

The most striking feature of CSDE dielectrics is that the internal generation of the dipole field is an immediate response to applied  $\vec{E}_G$  unlike in randomly incorporated dipoles that require an applied electric field with a certain threshold. Moreover, the embedded interfacial dipoles are far from the interface of the active layer; thus, the adverse effects of dipoles in the dielectric on the energetic disorder of the organic semiconductor<sup>13</sup> can be minimized. Even at extremely low  $V_G$  (e.g., below  $-0.5 \text{ V}$ ), the estimated power saving through voltage reduction could exceed 95% given the same level of charge current. The fabrication of FETs with superior *ss*, low off-state current, and low gate leakage current is highly essential for the reduction of power consumption. Here, we disregarded the charging current during switching (dynamic) and the off-state current (static) power consumption, both of which are important to a circuit. After more than six months of storage in an ambient air environment and long-term continuous operations, the OFETs continue to operate well and exhibit very sharp *ss* (below 100 mV/dec.) and very low off-state current (below  $10^{-11} \text{ A}$ ) (Fig. 6). This observation reflects the excellent controllability of the gate and the effect of the strong internal dipole field. Finally, we note that although the maximum capacitance and gate leakage current of the present CSDE dielectrics are not the best in the literature,<sup>17–23</sup> but above-mentioned feature allows enough capacitance for channel current flow at very low  $V_G$ , thus great FET performance especially in subthreshold characteristics. CSDE dielectrics can also be produced from other metals, such as titanium and tantalum, through the same approach discussed above. However, this idea requires further theoretical investigations.

### III Conclusions

A useful approach for hybrid bilayer dielectrics with an extremely large internal charged-state  $\vec{E}_{\text{dipole}}$  that enhances the applied external  $\vec{E}_G$  during device operations was demonstrated in this study. This dipole field facilitated the faster accumulation of sufficient charges within the active

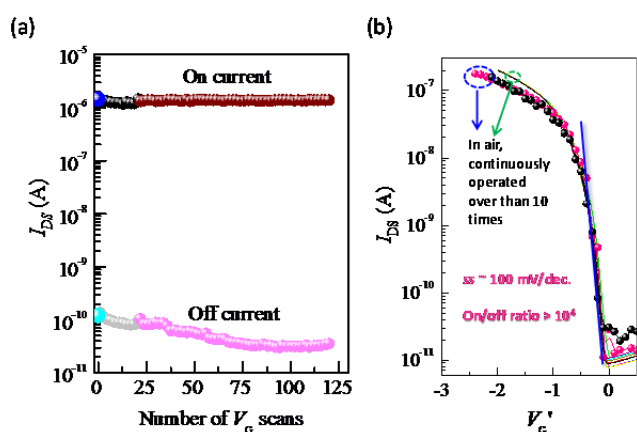


**Fig. 6.** Long-term stability of pentacene OFETs with CSDE dielectric in ambient air conditions. (a) Plot of output current ( $I_{DS}$ ) at on and off states versus number of gate voltage ( $V_G$ ) scans at  $V_D$  of -4 V. The on current was extracted from the transfer curve at constant effective gate voltage  $V_G' = V_G - V_{th}$ . (b) Comparison of transfer curves ( $V_D = -2V$ ) after hundreds of times of continuous operation and more than three months (lines) and six months (symbols) of storage in an ambient air environment (temperature = 25 °C; humidity = 40%).

channel of OFETs at very low supply voltage. The approach can be applied in low voltage-driven electronics. The integrated application of frequency-dependent  $\vec{P}-\vec{E}$  analysis and in situ charge-enhanced Raman scattering with quantum chemical calculations confirmed that the unusual electrical features of CSDE dielectrics are caused by the new species at the polymer/metal-oxide interface. The generated internal electric fields from CSDE dielectrics with a large right vector and fast response features allowed the pentacene OFETs to exhibit ultrahigh electrical performance at an extremely low operating voltage (field-effect mobility in the linear regime can achieve 1.5 cm<sup>2</sup>/Vs at only 0.1 V and 2.0 cm<sup>2</sup>/Vs at only 0.5 V), as well as excellent operational stability (superior switching and off characteristics were maintained even after long-term continuous operations and storage in air) under ambient air conditions. These results show an extremely good performance for OFETs operating in ambient air. Furthermore, a low-voltage driven polymer FET based on poly(3-hexylthiophene-2,5-diyl) (P3HT), which is a widely studied polymer semiconductor, with CSDE dielectric has also been successfully fabricated and tested in ambient air (ESI, Fig. S8†). Notably, the use of P3HT in OFETs in ambient air is known to suffer from a serious moisture problem, hence the very poor FET characteristics in the air.<sup>45</sup> This drawback can significantly be improved by employing the present art, but it still cannot be completely resolved. Further studies are also currently underway. Potential and general usage of CSDE dielectrics for other semiconductor-based FETs is still highly expected. In contrast to inorganic semiconductor-based FETs, we believe that the air-stable low-voltage driven FET concept is also feasible to organic FETs. The introduction of a charged-state dipole field into nanoscale dielectrics is an interesting concept for the fabrication of high-charge density capacitors and could have promising applications.

## IV Experimental Section

### A Sample preparation

An Al gate electrode 50 nm thick was e-gun evaporated through a steel mask onto a glass substrate. The gate electrode was then treated using oxygen plasma at 200 W power and 50 mbar pressure for 15 s, forming a thin AlO<sub>x</sub> layer with -OH and/or -O<sup>-</sup> surface active groups. Compared with native AlO<sub>x</sub> with a high water contact angle of approximately 60° to 70°,<sup>46</sup> the prepared AlO<sub>x</sub>-OH layer has a water contact angle of only 25°, confirming the result. A thermally cured crosslink-PVP layer was spin-coated from 1 wt% *n*-butanol solution with a blend of PVP ( $M_w$  of 22,000 g/mol) and PMF ( $M_w$  of 511 g/mol) at a 2:1 weight ratio and heated at 150 °C for 20 min to observe the CSDE dielectrics. For comparison, PVP:PMF at different weight ratios was also used to prepare the cross-linked PVP layers on the AlO<sub>x</sub> surface. Additionally, a 2 wt% *n*-butanol solution of PVP and PMF at a 2:1 weight ratio was used to observe CSDE dielectrics with thicker crosslink-PVP layer and crosslink-PVP/HfO<sub>2</sub> bilayer dielectrics. The preparation of HfO<sub>2</sub> layer upon the AlO<sub>x</sub> layer was described previously.<sup>47</sup> The PMMA buffer layer upon the AlO<sub>x</sub> layer was spin-coated from a 1 wt% anisole solution and heated at 150 °C for 20 min. The pentacene active layers (thickness of 60 nm) were then thermally evaporated (at a deposition rate of 0.5 Å/s and a vacuum level of 2 × 10<sup>-5</sup> torr) and patterned with a shadow mask to avoid unnecessary leakage current paths. Silver was deposited through the second shadow mask on the patterned pentacene surface and served as source and drain electrodes. The channel dimensions were 800 μm wide and 100 μm to 300 μm long. At least 15 devices were tested at each channel dimension. All chemical reagents were obtained commercially from Aldrich Chemical Co. and used as received.

### B Characterizations

The thickness of each layer was carefully calibrated with a J.A. Woollam Co. alpha-SE Ellipsometer. Surface free energy was analyzed through the OCA15 contact angle goniometer (Dataphysics Co.). All electric measurements were conducted under a dark shield box in ambient air. The polarization density and dielectric constant characterization of the MISM and MIM diodes were evaluated using an Agilent E4980 LCR meter. The FETs were characterized using a Keithley 4200-SCS and/or Keithley 2636. The  $\mu_{lin}$  and  $\mu_{sat}$  were extracted through the transconductance method and the standard FET model equation (i.e., plotted  $\sqrt{I_D}$  vs.  $V_G$ ), respectively.<sup>6</sup>

### C Quantum chemical calculations

The geometry of the PMF was first optimized using the density functional theory (DFT) at the B3LYP/6-31G(d) level of theory with periodic boundary conditions. Next, the dipole moments and Raman spectra of the interfacial species were calculated using our own *n*-layered integrated molecular orbital and molecular mechanics (ONIOM),<sup>48</sup> a two-layered approach widely used for large molecules. We considered a

repeat unit of optimized PMF with –OH, –O-Al, or –O-phenyl as the high layer [B3LYP/6-31G(d) level in theory] and formed a bond with the adjacent unit and with a phenol group of PVP in the low layer (HF/3-21G\* level in theory). All the calculations were performed using the Gaussian suite of programs.

### Acknowledgements

This work was supported by the National Science Council, Taiwan, through Grant NSC 101-2221-E-006-163-MY3 and NSC 98-2221-E-018-017. We are grateful to the National Center for High-performance computing of Taiwan for computer time and facilities. We acknowledge Prof. Chia-Jyi Liu, Department of Physics, National Chang-Hua University of Education, Taiwan, for their equipment support and cooperation.

### Notes and references

<sup>a</sup> Institute of Photonics, National ChangHua University of Education, Changhua 500, Taiwan

<sup>b</sup> Department of Photonics, Advanced Optoelectronic Technology Center, National Cheng Kung University, Tainan 701, Taiwan, Fax: +886 6 2095040 ; Tel: +886 6 2757575 63916 ; E-mail: [shlcheng@mail.ncku.edu.tw](mailto:shlcheng@mail.ncku.edu.tw)

<sup>c</sup> Department of Physics, National ChangHua University of Education, Changhua 500, Taiwan

Electronic Supplementary Information (ESI) available: Additional details and figures. See DOI: 10.1039/b000000x/

- J. Baxter, Z. Bian, G. Chen, D. Danielson, M. S. Dresselhaus, A. G. Fedorov, T. S. Fisher, C. W. Jones, E. Maginn, U. Kortshagen, A. Manthiram, A. Nozik, D. R. Rolison, T. Sands, L. Shi, D. Shollh and Y. Wu, *Energy Environ. Sci.*, 2009, **2**, 559.
- A. M. Ionescu and H. Riel, *Nature*, 2010, **479**, 329.
- L. C. Haspert, E. Gillette, S. B. Lee and G. W. Rubloff, *Energy Environ. Sci.*, 2013, **6**, 2578.
- D. R. Rolison, J. W. Long, J. C. Lytle, A. E. Fischer, C. P. Rhodes, T. M. McEvoy, M. E. Bourg and A. M. Lubers, *Chem. Soc. Rev.*, 2009, **38**, 226.
- K. Naoi, S. Ishimoto, J. Miyamoto and W. Naoi, *Energy Environ. Sci.*, 2012, **5**, 9363.
- Z. Bao and J. Locklin (eds), *Organic Field-Effect Transistors*, CRC press, Boca Raton, FL, 2007.
- D. L. Pulfrey, *Understanding Modern Transistors and Diodes*, Cambridge University Press, NY, 2010.
- C. Hu, *Int. Conf. Solid State Integr. Circuits Technol. Proc. ICSICT*, Beijing, China, Oct, 2008.
- V. Coropcean, J. Cornil, D. A. da Silva Filho, Y. Olivier, R. Silbey and J.-L. Brédas, *Chem. Rev.*, 2007, **107**, 926.
- R. P. Ortiz, A. Facchetti and T. J. Marks, *Chem. Rev.*, 2010, **110**, 205.
- H. Sirringhaus, *Adv. Mater.*, 2009, **21**, 3859.
- J. Veres, S. D. Ogier, S. W. Leeming, D. C. Cupertino and S. M. Khaffaf, *Adv. Funct. Mater.*, 2003, **13**, 199.
- T. Richards, M. Bird and H. Sirringhaus, *J. Chem. Phys.*, 2008, **128**, 234905.
- W. Xu, F. Wang and S.-W. Rhee, *J. Mater. Chem.* **2012**, **22**, 1482.
- M.-H. Yoon, C. Kim, A. Facchetti and T. J. Marks, *J. Am. Chem. Soc.*, 2006, **128**, 12851.
- H. L. Cheng, Y. S. Mai, W. Y. Chou, L. R. Chang and X. W. Liang, *Adv. Funct. Mater.*, 2007, **17**, 3639.
- M. Halik, H. Klauk, U. Zschieschang, G. Schmid, C. Dehm, M. Schütz, S. Maisch, F. Effenberger, M. Brunnbauer and F. Stellacci, *Nature*, 2004, **431**, 963.
- K. D. Kim and C. K. Song, *Appl. Phys. Lett.*, 2006, **88**, 233508.
- H. Klauk, U. Zschieschang, J. Pflaum and M. Halik, *Nature*, 2007, **445**, 745.
- T. Sekitani, U. Zschieschang, H. Klauk and T. Someya, *Nat. Mater.*, 2010, **9**, 1015.
- Y. Chung, E. Verploegen, A. Vailionis, Y. Sun, Y. Nishi, B. Murmann and Z. Bao, *Nano Lett.*, 2011, **11**, 1161.
- M. E. Roberts, N. Queraltó, S. C. B. Mannsfeld, B. N. Reinecke, W. Knoll and Z. Bao, *Chem. Mater.*, 2009, **21**, 2292.
- S. H. Kim, K. Hong, W. Xie, K. H. Lee, S. Zhang, T. P. Lodge and C. D. Frisbie, *Adv. Mater.*, 2013, **25**, 1822.
- V. R. Rai, V. Vandalon and S. Agarwal, *Langmuir*, 2010, **26**, 13732.
- A. Gerber, H. Kohlstedt, M. Fitsilis, R. Waser, T. J. Reece, S. Ducharme and E. Rije, *J. Appl. Phys.*, 2006, **100**, 024110.
- S. C. Lim, S. H. Kim, J. B. Koo, J. H. Lee, C. H. Ku, Y. S. Yang and T. Zyung, *Appl. Phys. Lett.* 2007, **90**, 173512.
- S. H. Jeong, C. K. Song and M. Yi, *Appl. Phys. Lett.* 2009, **94**, 183302.
- G. G. Raju, *Dielectrics in Electric Fields*, Marcel Dekker, Inc., NY, 2003.
- C. H. Kim, O. Yaghmazadeh, D. Tondelier, Y. B. Jeong, Y. Bonnasieux and G. Horowitz, *J. Appl. Phys.*, 2011, **109**, 083710.
- S. E. Fritz, T. W. Kelley and C. D. Frisbie, *J. Phys. Chem. B*, 2005, **109**, 10574.
- M. E. Gershenson, V. Podzorov and A. F. Morpurgo, *Rev. Mod. Phys.*, 2006, **78**, 973.
- S. Kera, H. Yamane and N. Ueno, *Prog. Surf. Sci.*, 2009, **84**, 135.
- H. L. Cheng, Y. S. Mai, W. Y. Chou and L. R. Chang, *Appl. Phys. Lett.*, 2007, **90**, 171926.
- D. J. Gundlach, L. Jia and T. N. Jackson, *IEEE Electron Device Lett.*, 2001, **22**, 571.
- L. Shang, Z. Ji, H. Wang, Y. Chen, X. Liu, M. Han and M. Liu, *IEEE Electron Device Lett.*, 2011, **32**, 1451.
- S. H. Kim, S. Nam, J. Jang, K. Hong, C. Yang, D. S. Chung, C. E. Park and W. S. Choi, *J. Appl. Phys.*, 2009, **105**, 104509.
- K. D. Kim and C. K. Song, *Jpn. J. Appl. Phys.*, 2010, **49**, 111603.
- J.-M. Choi, D. K. Hwang, S. H. Jeong, J. H. Park, E. Kim, J. H. Kim and S. Im, *J. Electrochem. Soc.*, 2007, **154**, H331.
- H. Klauk, M. Halik, U. Zschieschang, G. Schmid, W. Radlik and W. Weber, *J. Appl. Phys.*, 2002, **92**, 5259.
- H. E. Katz, X. M. Hong, A. Dodabalapur and R. Sarpeshkar, *J. Appl. Phys.*, 2002, **91**, 1572.
- G. Gu, M. G. Kane, J. E. Doty and A. H. Firester, *Appl. Phys. Lett.*, 2005, **87**, 243512.
- R. Parashkov, E. Becker, G. Ginev, T. Riedl, H.-H. Johannes and W. Kowalsky, *J. Appl. Phys.*, 2004, **95**, 1594.
- Y. Jang, D. H. Kim, Y. D. Park, J. H. Cho, M. Hwang and K. Choa, A., *Appl. Phys. Lett.*, 2005, **87**, 152105.

- 44 D. K. Hwang, M. S. Oh, J. M. Hwang, J. H. Kim and S. Im, *Appl. Phys. Lett.*, 2008, **92**, 013304.
- 45 S. Hoshino, M. Yoshida, S. Uemura, T. Kodzasa, N. Takada, T. Kamata and K. Yase, *J. Appl. Phys.*, 2004, **95**, 5088.
- 46 V. Safonov, A. Zykova, J. Smolik, R. Rogovska, N. Donkov and V. Georgieva, *J. Phys.: Conf. Ser.*, 2010, **253**, 012068.
- 47 B. L. Yeh, Y. H. Chen, L. Y. Chiu, J. W. Lin, W. Y. Chen, J. S. Chen, T. H. Chou, W. Y. Chou, F. C. Tang and H. L. Cheng, *J. Electrochem. Soc.*, 2011, **158**, H277.
- 48 S. Dapprich, I. Komáromi, K. S. Byun, K. Morokuma and M. J. Frisch, *J. Mol. Struct. (Theochem)*, 1999, **462**, 1.46